Surfaces and Interfaces 87 (2026) 108933

Contents lists available at ScienceDirect

Surfaces and Interfaces

journal homepage: www.sciencedirect.com/journal/surfaces-and-interfaces

Electrospun thermoplastic polyurethane fibers functionalized with MOFs and Ag nanocubes for enhanced VOC detection

Chien-Lin Huang [a,*], Yi-Chen Lin [a], Kai-Wun Chen [a], Yin-Hsuan Chang [b], Ming-Chung Wu [b,c,d], Su-Wen Hsu [e]

[a] Department of Fiber and Composite Materials, Feng Chia University, No. 100, Wenhua Rd., Xitun Dist., Taichung City, Taiwan (R.O.C.), Taichung 407102, Taiwan
[b] Department of Chemical and Materials Engineering, Chang Gung University, No.259, Wenhua 1st Rd., Guishan Dist., Taoyuan City, Taiwan (R.O.C.), Taoyuan 333323, Taiwan
[c] Center for Sustainability and Energy Technologies, Chang Gung University, No.259, Wenhua 1st Rd., Guishan Dist., Taoyuan City, Taiwan (R.O.C.), Taoyuan 333323, Taiwan
[d] Division of Neonatology, Department of Pediatrics, Chang Gung Memorial Hospital, No. 5, Fuxing St., Guishan Dist., Taoyuan City, Taiwan (R.O.C.), Linkou, Taoyuan, 333423, Taiwan
[e] Department of Chemical Engineering, Nation Cheng Kung University, No.1, University Road, Tainan City, Taiwan (R.O.C), Tainan 701401, Taiwan

ARTICLE INFO

Keywords:
Volatile organic compounds
Thermoplastic polyurethane
Electrospinning
UiO-66
Silver nanocubes
Surface plasmon resonance

ABSTRACT

Timely volatile organic compounds (VOCs) detection is essential for environmental monitoring and disease diagnostics, spurring advances in affordable, real-time sensors. A metal-organic frameworks (UiO-66) and silver nanocubes (AgNCs) were incorporated into electrospun thermoplastic polyurethane (TPU) nanofibers to enhance the adsorption and optical sensing of VOCs, such as acetone and isopropanol. Composite fibrous films were prepared by two methods: direct blending of UiO-66 nanoparticles into the TPU solution prior to electrospinning, and ultrasonic treatment, which randomly anchored UiO-66 and AgNC nanoparticles onto TPU fibers. VOC adsorption on these TPU composite fibers induced measurable UV–vis extinction shifts. Ultrasonic treatment enhanced the extinction response by anchoring UiO-66 and AgNCs on the fiber surface, preventing their encapsulation beneath TPU chains. Surface-exposed UiO-66 improved VOC adsorption, while plasmon resonance from AgNCs amplified light scattering, thereby increasing optical sensitivity. In contrast, direct blending resulted in TPU/UiO-66 composite fibers where TPU likely covered UiO-66 nanoparticles, reducing their accessibility and adsorption capacity, leading to no significant enhancement in extinction response. The TPU-UiO-66-AgNC composite fibrous films exhibited a detection limit of 50 ppm for acetone vapors, confirming their suitability for VOC sensing applications. Additionally, the optical response behavior of the TPU composite fibrous films was modeled using modified pseudo-first-order and pseudo-second-order equations to elucidate the adsorption mechanisms and kinetics of VOC uptake.

1. Introduction

Real-time volatile organic compounds (VOCs) detection is crucial for pollution control and early disease diagnosis [1–3]. Although conventional methods such as gas chromatography-mass spectrometry and proton-transfer-reaction mass spectrometry offer high accuracy for detecting low-concentration VOCs, they are often expensive and time-consuming [1,4]. Therefore, the development of low-cost, real--time VOC sensors has garnered significant research interest. Among these, optical sensors have emerged as promising candidates due to their simple device architecture, which typically consists of a sensing material integrated with a substrate, and the ease of material fabrication.

Electrospun polymer nanofibers, characterized by high surface area, porous structure, and excellent permeability, have shown great potential in chemical sensing, and VOC adsorption [5–7]. Wu et al. [8,9] investigated electrospun Poly(methyl methacrylate) (PMMA)/ poly (3-hexylthiophene) (P3HT) and PMMA/CdSe-CdS/Ag nanofiber membranes for VOC sensing chip development. The high surface area and circular geometry of electrospun fibers facilitate proportional optical responses, such as extinction changes, upon VOC adsorption. These findings demonstrate the feasibility and cost-effectiveness of optical VOC detection.

* Corresponding author.
E-mail address: clhuang@mail.fcu.edu.tw (C.-L. Huang).

https://doi.org/10.1016/j.surfin.2026.108933
Received 26 August 2025; Received in revised form 18 January 2026; Accepted 4 March 2026
Available online 7 March 2026

Thermoplastic polyurethane (TPU) is a versatile material known for its flexibility, biocompatibility, hydrolytic stability, transparency, flame retardancy, and antistatic properties. Its excellent elongation makes it ideal for flexible sensors with strong detection capabilities [10,11]. TPU fibers significantly adsorb VOCs and, with their reversible shape memory effect, offer easy adsorption and release, making TPU fiber membranes reusable and efficient for filtration. Scholten *et al.* [11] showed that electrospun TPU fibers effectively absorb VOCs, similar to activated carbon. TPU fibers can also be desorbed through temperature and pressure changes, making them reusable. Wang *et al.* [12] produced core-sheath fibers with PAN in the core and TPU in the sheath via coaxial electrospinning. The PAN fibers' surface was coated with MCM-41 molecular sieves using TPU functional groups. These composite fibers effectively removed low-concentration acetone from indoor air. The above findings suggest that electrospun TPU fibers are promising candidate substrates for VOC adsorption. However, to develop an effective strategy, it is crucial to efficiently integrate high-porosity, high-specific surface area nanoparticles onto the surface of the electrospun TPU fibers in a rapid and cost-effective way, thereby enhancing the sensitivity of VOC sensors.

Metal-organic frameworks (MOFs) are crystalline materials composed of metal ions or clusters coordinated to organic linkers, forming a three-dimensional porous network, which is promising for gas sensing [13–15]. UiO-66 is a zirconium-based MOF consistsed of $Zr_6O_4(OH)_4$ nodes linked by 12 benzenedicarboxylic acid (BDC) linkers, forming a cubic structure with micropores that have triangular windows [14]. While many MOFs suffer from poor hydrothermal stability, which restricts their application in humid environments, UiO-66 demonstrates superior hydrothermal and acid resistance owing to its highly robust structure and strong Zr(IV)–oxygen coordination bonds [16]. Ou *et al.* optimized the structural properties of UiO-66 for selective adsorption of benzene and toluene [17]. Yu *et al.* investigated ZIF-7, UiO-66, and MOF-5 for selective adsorption of VOCs from human breath, identifying UiO-66 as the most effective, particularly for acetone and isopropanol (IPA) [18]. Accordingly, this study employs UiO-66 to enhance the VOC adsorption performance of electrospun TPU fibers.

Plasmonic nanocrystals such as silver nanocubes (AgNCs) exhibit strong surface plasmon resonance (SPR), which is highly dependent on their size, geometry, and dielectric environment [19,20]. SPR arises from the collective oscillation of conduction electrons upon interaction with incident light, enhancing local electromagnetic fields. Coupling between nanocrystals and adjacent optically active media further amplifies optical responses, including visible absorption and Raman scattering. These properties make plasmonic materials attractive for compact, room-temperature sensors and other nanophotonic applications [21]. Previous studies embedded Ag nanoparticles (AgNPs) in PMMA nanofibers [20,22,23], where they were completely encapsulated by the polymer, yet still significantly enhanced light scattering due to their visible-range plasmonic response, thereby increasing gas sensing sensitivity. In this study, AgNCs with sharp corners were anchored onto TPU fiber surfaces to leverage their strong SPR effects and enhance VOC-induced optical extinction changes, thereby improving sensor sensitivity.

Fiber surface functionalization can be achieved without the need for UV-ozone treatment [20,22,23], chemical grafting [24], or in situ MOF growth to enhance surface area or porosity [25]. Instead, a simple ultrasonic bath treatment allows nanoparticles to be embedded onto electrospun TPU fibers by immersing them in a nanoparticle aqueous solution for a short duration. This method enables tunable surface activity by selecting different MOFs, offering selective VOC adsorption. Compared to conventional methods, it is faster, more cost-effective, and scalable for surface modification of electrospun fibers. In this study, UiO-66 and silver nanocubes (AgNCs) were employed as functional nanoparticles to enhance the performance of electrospun TPU fibers for VOC optical sensing. UiO-66 served to increase local VOC adsorption due to its high surface area and affinity for polar molecules, while AgNCs enhanced optical scattering through SPR [26]. A cost-effective approach was used to integrate these nanoparticles with TPU fibers, aiming to enhance detection sensitivity and lower the detection limit. Composite fibrous films were fabricated via two approaches: (1) direct blending of UiO-66 nanoparticles into the TPU solution prior to electrospinning; and (2) ultrasonic-assisted surface anchored UiO-66 and AgNC nanoparticles onto electrospun TPU fibers. Results indicated that anchoring UiO-66 nanoparticles on TPU fibers enhanced acetone vapor adsorption, while AgNCs contributed to an amplified optical response. Additionally, the extinction changes in the TPU-UiO-66-AgNC composite fibrous films were positively correlated with VOC adsorption, lowering the detection limit to 50 ppm. Adsorption behavior was analyzed using modified pseudo-first-order (PFO) and pseudo-second-order (PSO) kinetic models to elucidate underlying mechanisms.

2. Experimental

2.1. Materials

TPU pellets were supplied by Evermore Chemical Inductrial Co. LTD. (EMH-85A-1, Taichung, Taiwan). Zirconium (IV) chloride and ortho-Dichlorobenzene (*o*DCB) were purchased from Acros Organics. BDC was purchased from Showa Chemical Co. LTD. Acetone, Dimethylformamide (DMF), tetrahydrofuran (THF), toluene, ethanol, and IPA was purchased from Echo Chemical Co. (Miaoli, Taiwan). Polyvinylpyrolidone (PVP) with a weight-average molecular weight of 40,000 g/mol, were purchased from Alfa Aesar.

2.2. Synthesis of UiO-66 and AgNC

UiO-66 was synthesized via a solvothermal method. $ZrCl_4$ (466 mg, 2 mmol) and terephthalic acid (199.2 mg, 1.2 mmol) was stirred with 120mL of DMF by using a 250 mL spherical reaction flask. Subsequently, the mixture was heated to 120 °C in an oil bath for 24 h. The resulting suspension was centrifuged to separate the products. The precipitated UiO-66 powders were filtered and then washed with ethanol. The product was dried in a vacuum oven at 120 °C for 24 h.

AgNCs were synthesized via a reported polyol method [27]. $AgNO_3$ and $CuCl_2$ were dissolved in 1,5-pentanediol as one precursor; PVP in 1, 5-pentanediol formed another. Both were injected alternately into 193 °C pentanediol—$AgNO_3$ at 500 μL/min and PVP at 320 μL/30 s. Post-synthesis purification (450 nm and 220 nm filtration) reduced shape impurities from ~20 % to <5 %. The resulting AgNCs averaged 109 ± 7 nm in size.

2.3. TPU composite fibrous films preparation

A 24 wt. % TPU solution was prepared in DMF and electrospun at room temperature using a needle (D_i/D_o/length = 0.69 mm/1.07 mm/40 mm). Electrospinning was performed at 0.3 mL/h and 13.5 kV with a 14 cm needle-to-collector distance. Fibers were collected on a 10 cm rotating aluminum drum (540 rpm). Glass slides attached to the collector served as VOC-sensing substrates, with TPU nanofibers deposited at 0.247 ± 0.044 mg/cm^2.

AgNCs were dispersed in ethanol to form a colloidal solution (max extinction: 1.44 at 589 nm) and diluted 30-fold. This was further diluted 2–20 times with deionized water to prepare TPU-AgNC composite fibrous films. Separately, UiO-66 nanoparticles were ultrasonically dispersed in water for 10 minutes using an ultrasonic bath (Delta DC200H; frequency 40 kHz, output power 200 W). Electrospun TPU fibers on glass slides were immersed in UiO-66 and AgNC solutions of varying concentrations, then ultrasonicated for 2 minutes to produce TPU-UiO-66, TPU-AgNC, and TPU-UiO-66-AgNC composites. The TPU composite fibers for the extinction spectrum test were heat-treated at 120 °C for 1 h in a vacuum oven, followed by air cooling to room temperature. Samples were labeled TPU-UiO-66-X (X wt % UiO-66) and

TPU-AgNC-dX (AgNC diluted X times).

2.4. Morphology and characterization of UiO-66, AgNC, and fibers

Fiber morphology was examined via SEM (Hitachi S4100, 3 kV), and average diameters were calculated from 200 fibers. UiO-66 morphology was observed by TEM (Jeol JEM-1200EX). FTIR spectra (Perkin-Elmer Spectrum Two) were recorded with 32 scans at 2 cm^{-1} resolution. TGA (TGA2950) and DSC (TA Q20) analyses were conducted under nitrogen. WAXD profiles were obtained using a Bruker NanoSTAR diffractometer, and UiO-66 surface areas were measured with BET analysis (ASAP 2020).

2.5. Optical measurement (Extinction Spectrum)

A quartz chamber (4.5 × 4.0 × 4.5 cm^3) was filled with varying VOCs until fully evaporated, then TPU composite fibrous films were placed inside. Extinction spectra (400–1000 nm) were recorded using a UV-Vis spectrometer (Jasco V-730) [8,20]. VOC detection was performed at room temperature (25 °C) under a relative humidity of approximately 60 %. Sensitivity was evaluated via ΔE at 455 nm before and after VOC exposure.

The extinction formula is defined as follows [20]

$$\Delta E = E_t - E_{t_0} \tag{1}$$

where the extinction intensity of the peak before the VOC detection experiment is represented by E_{t_0}, while the extinction intensity of the peak after the experiment is represented by E_t.

3. Results and discussion

TPU-based composite fibrous films were fabricated via two approaches as illustrated in Fig. 1: (1) direct blending of UiO-66 into the TPU solution prior to electrospinning (TPU/UiO-66); and (2) ultrasonic-assisted surface anchoring of UiO-66 and AgNCs onto electrospun TPU fibers (TPU-UiO-66, TPU-AgNC, and TPU-UiO-66-AgNC), yielding surface-functionalized composite films. These two strategies were adopted to compare the effect of nanoparticle distribution on VOC adsorption and optical sensing performance. The ultrasonic-assisted anchoring approach presumably provides more accessible surface-exposed active sites and better preservation of nanoparticle functionality, which is advantageous for VOC sensing.

Fig. 2(a and b) displays SEM images of electrospun TPU fibers before and after thermal treatment. TPU fibers exhibit a bead-free morphology with a uniform diameter distribution and well-stretched polymer chain network. Following thermal annealing at 120 °C for 1 h in a vacuum oven, the fiber morphology was well preserved, with the surfaces appearing smoother. The average fiber diameter after thermal treatment increased slightly. These results indicate that the thermal treatment had minimal impact on the overall fiber structure and morphology of neat TPU fibers. Fig. 2(c) shows DSC traces of TPU cast films and as-spun fibers, revealing two melting peaks: T_{m1} (single hard segment disordering) and T_{m2} (hard microphase melting) [11,28] To avoid vapor adsorption interference, TPU fibers were thermally treated at 120 °C (below T_{m2}) for 1 hr. Fig. 2(d) shows FTIR spectra of TPU films and fibers. Carbonyl stretching bands (1760–1600 cm^{-1}) were deconvoluted into four peaks [Fig. 2e and f]: free urethane (1732 cm^{-1}), H-bonded urethane (1706 cm^{-1}), free urea (1676 cm^{-1}), and H-bonded urea (1658 cm^{-1}) [29]. Hydrogen bonding index ($HBI_{(C=O)}$) was calculated accordingly [29].

$$HBI_{(c=O)} = \frac{A_{1706} + A_{1658}}{A_{1706} + A_{1658} + A_{1732} + A_{1676}} \times 100\% \tag{2}$$

where $HBI_{(C=O)}$ is the extent of carbonyl absorption groups participating in hydrogen bonding, A_{1732}, A_{1706}, A_{1676}, and A_{1658} is the areas of the 1732, 1706, 1676, and 1658 cm^{-1} bands, respectively. The $HBI_{(C=O)}$ values for TPU cast films and fibers were 61.6 % and 49.5 %, respectively, indicating more free carbonyl groups in fibers. Solvent evaporation without external force in cast films preserves chain compactness, while electrospinning stretches TPU chains, reducing hydrogen bonding. These free carbonyl groups in fibers aid polar VOC adsorption.

Pereira et al. reported $HBI_{(C=O)}$ values of 54.2 % and 54.7 % for TPUs composed of IPDI hard segments and poly(caprolactone diol) (PCL) soft segments of shorter and longer chain lengths, respectively [29]. The $HBI_{(C=O)}$ values observed in our TPU cast films and electrospun fibers fall within this range. Theron et al. studied electrospun medical-grade TPU fibers and estimated an $HBI_{(C=O)}$ of ~69.5 % based on the 1703/1730 cm^{-1} FTIR absorbance ratio [30], highlighting the influence of TPU backbone chemistry on hydrogen bonding. Wang et al. also showed that stretching TPU reduces the degree of hydrogen bond formation [31], in agreement with our results.

The TEM images of UiO-66 [Fig. 3a] exhibited cubic and intergrown crystals, averaging 128 ± 7 nm. Across batches, particle sizes varied slightly (60–135 nm), but all maintained consistent shapes and a standard deviation within 10 nm. WAXD peaks at 7.24° and 8.44° corresponded to (111) and (002) planes [Fig. 3b]. The diffraction peaks of UiO-66 were well fitted the simulated pattern [14,32,33]. Fig. 3(c) presents the FTIR spectra of UiO-66. The broad band near 3400 cm^{-1} corresponds to O–H stretching, indicative of adsorbed water within the pores. Peaks at 1577 and 1400 cm^{-1} are attributed to C=O stretching of the carboxylate ligands [32]. The band at 552 cm^{-1} corresponds to the asymmetric Zr–(OC) stretch [34], while peaks at 747 and 667 cm^{-1} are

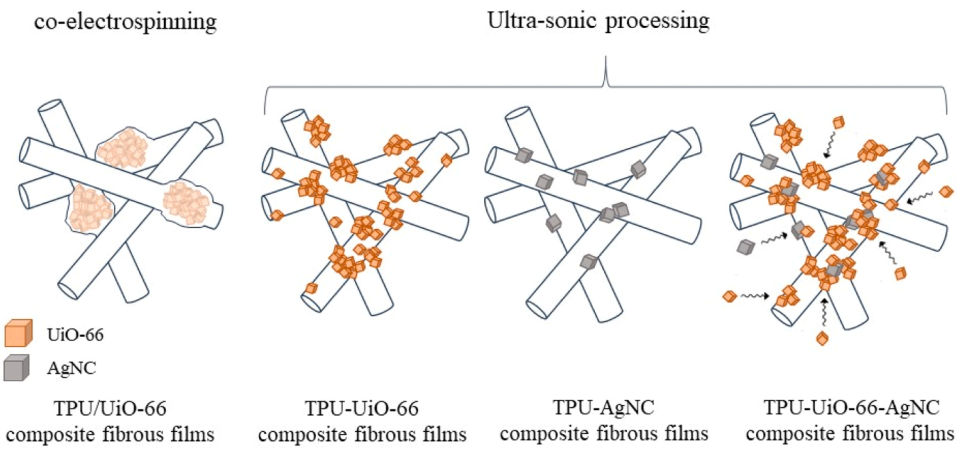

Fig. 1. Schematic representation of the TPU Composite fibrous films for VOC detection.

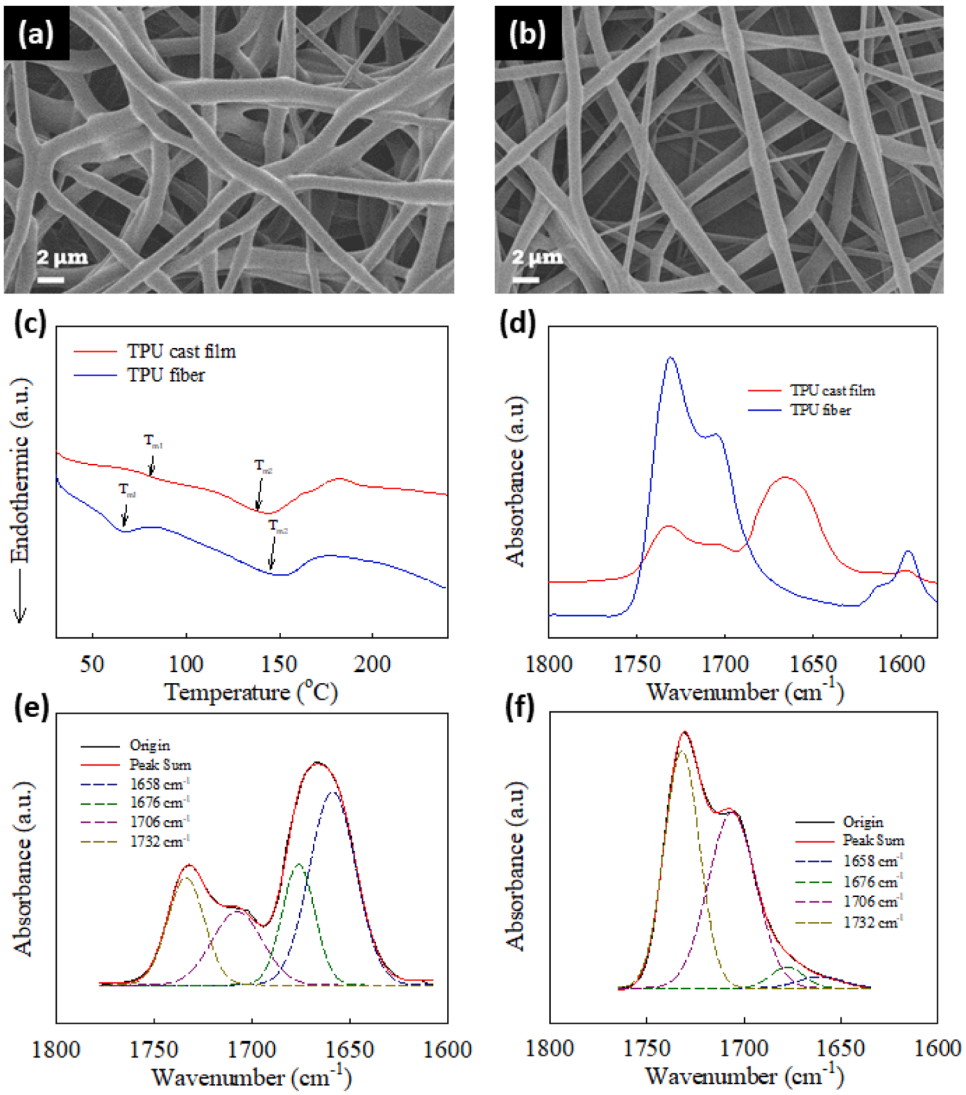

Fig. 2. SEM images of electrospun TPU fibers (a) before and (b) after thermal treatment. (c) DSC thermogram and (d) FTIR spectrum of TPU fiber. Deconvolution of the FTIR spectra of (e) TPU fiber and (f) TPU film at 1780 - 1620 cm^{-1}.

assigned to hydroxyl bending and μ_3-O stretching modes of the Zr–O cluster, respectively [32,34,35]. Fig. 3(d) presents nitrogen adsorption isotherms exhibiting Type I behavior, characteristic of microporous materials. The BET surface area was measured at 875.5 m^2/g, slightly lower than previously reported values [17], likely due to intergrown crystal domains limiting accessible surface area. The pronounced adsorption increase at low relative pressures further confirms a dominant microporous structure. These results collectively verify the successful synthesis of UiO-66 nanoparticles. Fig. 3(e) shows TEM images of AgNCs, revealing predominantly cubic shapes with minor irregular polyhedra. The average size of AgNCs was 109 ± 7 nm, smaller than UiO-66 particles. UV-Vis spectra [Fig. 3f] of diluted AgNC solutions displayed characteristic peaks at 353, 401, 484, and 574 nm. The sharp, intense peak at 484 nm corresponds to the plasmonic quadrupole mode, while the broader, less intense 574 nm peak is attributed to the plasmonic dipole mode. These features confirm the optical activity of AgNCs relevant to plasmon-enhanced sensing applications.

TEM images (Figure S1) show that incorporating UiO-66 into TPU nanofibers resulted in rougher surfaces with irregular protrusions, indicating UiO-66 aggregates coated by TPU. As shown in Fig. 4(a), the ΔE of TPU/UiO-66 composite films exposed to 300 ppm acetone vapor was only slightly higher than that of neat TPU fibers, suggesting similar adsorption behavior. The TPU chains likely covered the UiO-66 particles, limiting their adsorption capacity.

To improve VOC adsorption, ultrasonic-assisted surface anchoring was used to anchor UiO-66 and AgNC nanoparticles directly onto TPU fibers, preventing encapsulation by polymer chains and allowing unobstructed VOC interaction. Fig. 4(a and b) shows ΔE changes of TPU-UiO-66 and TPU-AgNC composite films exposed to 300 ppm acetone vapor. ΔE increased with UiO-66 content, confirming improved vapor adsorption from surface-anchored UiO-66, unlike internalized fillers in electrospun TPU/UiO-66, which were blocked by TPU chains. In contrast, TPU-AgNC films (d10, d5, d2) showed SPR-enhanced extinction, but high AgNC content, especially in d2, blocked surface sites, reducing acetone adsorption and lowering ΔE saturation versus neat TPU fibers.

Figures S2(a–b) show TGA curves of TPU-UiO-66 and TPU-AgNC fibers in nitrogen. TPU-UiO-66 remained stable from 100–500 °C, with a sharp mass loss near 500 °C due to decomposition of UiO-66's organic linkers, consistent with previous findings [14]. For TPU-AgNC fibers, 5 % weight loss began at 315 °C (neat TPU), 308 °C (d10), and 312 °C (d5). Higher AgNC content slightly raised decomposition onset but remained below that of neat TPU. Fig. 4(c and d) display SEM images of intergrown UiO-66 clusters and aggregated AgNCs anchored onto TPU-UiO-66-0.5 and TPU-AgNC-d5 fibers, respectively, via ultrasonication. Gao et al. [36] reported that graphite nanoplatelets (GNPs)

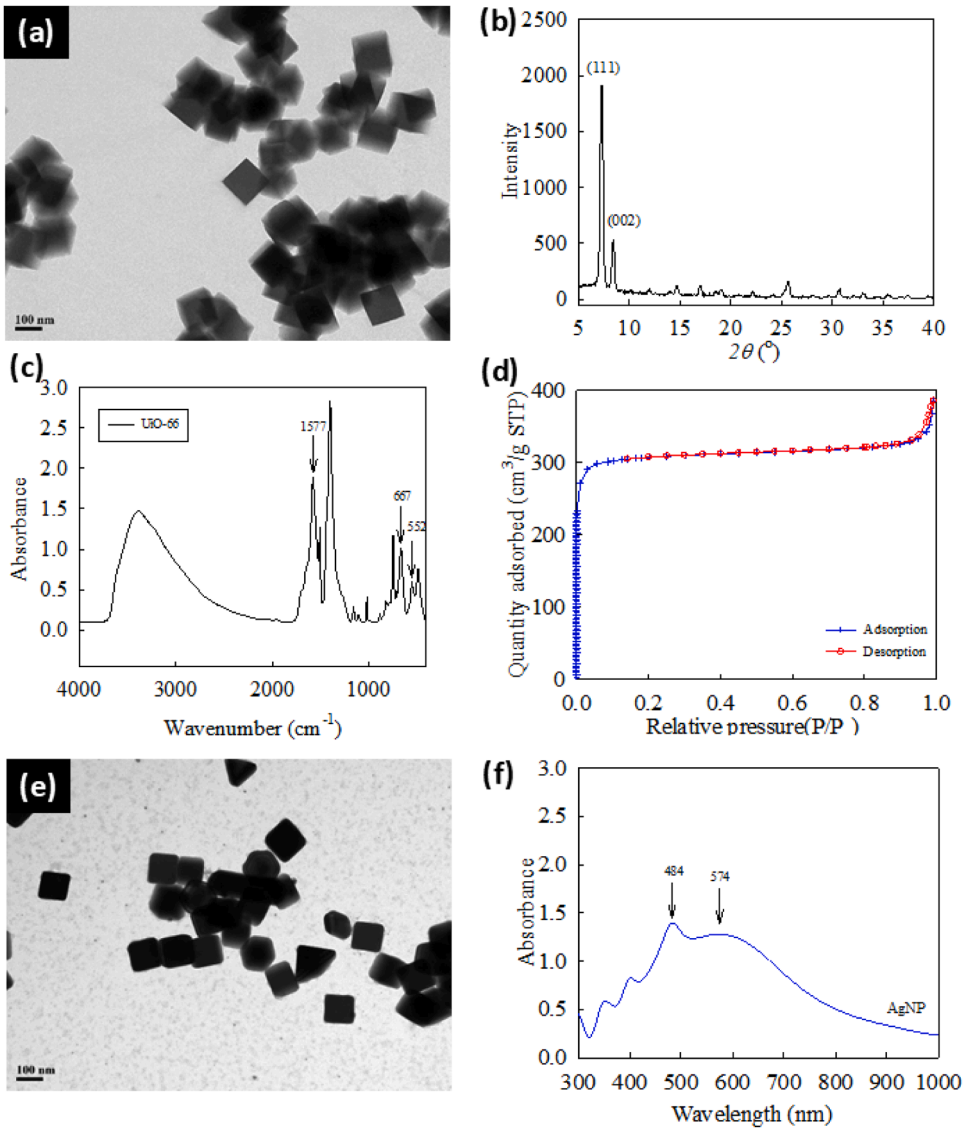

Fig. 3. (a) TEM image, (b) XRD pattern, (c) FTIR spectrum and (d) BET surface area analysis of synthesized UiO-66 nanoparticles. (e) TEM image and (f) UV spectrum of synthesized AgNC.

could be anchored or embedded onto TPU fibers through ultrasonic treatment. Building on this method, we applied a similar strategy to decorate TPU fiber surfaces with UiO-66 and AgNC nanoparticles. During ultrasonication, cavitation bubbles collapsed near the UiO-66 and AgNC particles, producing microjets and shock waves. These effects locally softened the TPU at the nanoparticle impact sites, enabling the nanoparticles to embed in the fiber. As a result, UiO-66 nanoparticles were randomly dispersed on the fiber surfaces, while AgNCs (109 ± 7 nm in diameter) were partially embedded with an average penetration depth of ~17 nm, confirming successful surface anchoring.

Figures S3 display SEM images of TPU-UiO-66 and TPU-AgNC composite fibers before and after thermal treatment. Post-annealing at 120 °C for 1 hour, UiO-66 nanoparticles (~143 nm) exhibited an increased embedding depth of ~28 nm, while AgNCs penetrated ~40 nm into the TPU matrix. This embedding enhancement is attributed to the thermal softening of TPU's amorphous regions, which facilitates chain mobility. These observations are consistent with findings by Jhang et al. [26], confirming that thermal treatment promotes nanoparticle incorporation into polymer fibers. The process is driven by thermodynamic factors such as surface energy minimization, favorable polymer–nanoparticle interactions, and polymer chain mobility, which collectively facilitate nanoparticle diffusion into the matrix [37].

Although the ΔE saturation values of TPU-UiO-66-1.0 and TPU-UiO-66-0.5 films were comparable, their response curves exhibited slight variations. As shown in Figure S4(a), excessive UiO-66 loading in TPU-UiO-66-1.0 led to nanoparticle aggregation on the fiber surface. This overloading exceeded the available acetone for adsorption, limiting further enhancement in light scattering and ΔE. These results suggest that TPU-UiO-66-0.5 provides more optimal sensing performance below 300 ppm acetone. Similarly, the SEM image in Figure S4(b) shows that TPU-AgNC-d2 exhibited surface blockage due to excessive AgNC loading, which suppressed the ΔE response, whereas TPU-AgNC-d5 achieved an optimal balance for effective acetone detection at 300 ppm.

Based on the characterization of TPU-UiO-66 and TPU-AgNC composite fibrous films, both UiO-66 and AgNC nanoparticles anchored on the TPU fiber surfaces contributed to enhancing the extinction change of TPU fibrous films. Consequently, a mixed solution containing 0.5 wt % UiO-66 and AgNCs diluted fivefold was prepared for ultrasonic-assisted surface decoration of TPU fibers. Fig. 5(a) show SEM images of TPU fiber surfaces after ultrasonication and thermal treatment, where UiO-66 and AgNC nanoparticles are irregularly anchored. Fig. 5(b) present corresponding SEM-EDX mapping, highlighting UiO-66 (green) and AgNC

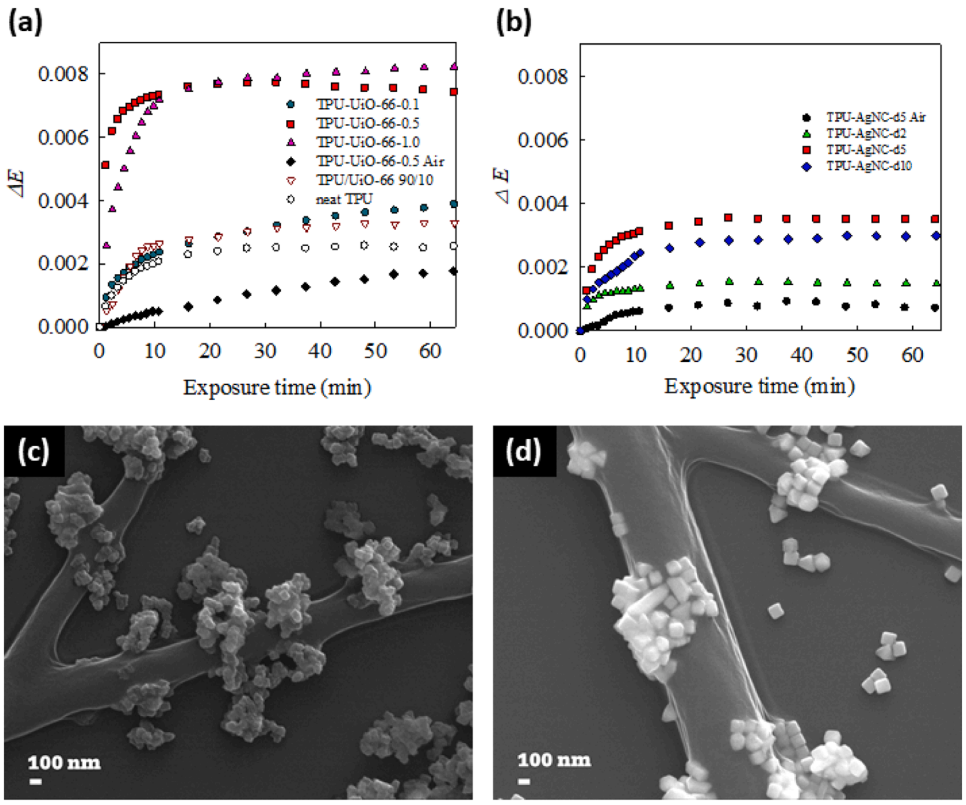

Fig. 4. Extinction changes of (a) neat TPU, TPU/UiO-66, TPU-UiO-66, and (b) TPU-AgNC films under 300 ppm acetone vapors; SEM images of (c) TPU-UiO-66-0.5 and (d) TPU-AgNC-d5 composite fibers.

(red) locations. Several AgNCs appear adjacent to or atop UiO-66 particles, indicating close spatial distribution achieved via ultrasonic treatment.

Fig. 5(c) shows that the ΔE of TPU-UiO-66-AgNC films reached ~4.7× that of neat TPU under 300 ppm acetone vapor. Despite random nanoparticle distribution, the composite outperformed TPU-UiO-66 and TPU-AgNC, due to synergistic effects: UiO-66 enhanced adsorption, and AgNCs amplified optical response via SPR. Figure S5 shows the ΔE variation of various TPU-UiO-66-AgNC composite fibrous films exposed to 300 ppm acetone vapors. all samples display a similar ΔE increase, saturating after ~10 minutes. The average saturation value (0.0104 ± 0.0012) demonstrates good measurement stability and reproducibility. Minor variations are attributed to differences in nanoparticle loading during ultrasonic anchoring. Fig. 5(d) shows that ΔE saturation of TPU-UiO-66-AgNC films peaked at 300 ppm acetone and declined with lower concentrations. At 25 ppm, ΔE was only slightly above air, suggesting possible interference from air. To ensure reliability, the minimum detectable concentration of acetone vapors for these films was set at 50 ppm.

The ΔE curve of TPU composite fibrous films during acetone vapor adsorption follows an exponential trend resembling the Avrami equation [38]. Gas adsorption in porous materials typically follows physical or chemical mechanisms, modeled by PFO and PSO kinetics [38–41]. PFO describes physical adsorption (Eq. 3), while PSO reflects chemical adsorption (Eq. 4).

$$q_t = Q_s\left(1 - e^{(-K_1 t)}\right) \tag{3}$$

$$q_t = \frac{\left(K_2 {Q_s}^2 t\right)}{\left(1 + K_2 Q_s t\right)} \tag{4}$$

where q_t is the adsorbed gas at time t (mL), Q_s is the saturated adsorption (mL), K_1 and K_2 are the equilibrium constants for the PFO (min^{-1}) and PSO model (mL^{-1} min^{-1}) models, respectively, and t is time (min).

In this study, the ΔE variation over time for TPU composite fibrous films differs from the gas adsorption amount (q_t) as described in the PFO and PSO models. Nevertheless, because the ΔE variation results from the change in the refractive index around the TPU composite fibers after adsorbing VOC gases, which in turn affects the light intensity detected by the UV-vis detector, it can be inferred that the ΔE variation over time (ΔE_t) is likely positively correlated with q_t. Consequently, by substituting ΔE_t and ΔE saturation value (ΔE_s) for q_t and Q_s in Eq. (3) and Eq. (4), Eqs. (5) and (6) are obtained, respectively.

$$\Delta E_t = \Delta E_s\left(1 - e^{(-K_1 t)}\right) \tag{5}$$

$$\Delta E_t = \frac{\left(K_2 {\Delta E_s}^2 t\right)}{\left(1 + K_2 \Delta E_s t\right)} \tag{6}$$

Fig. 5(c) also shows the linear fitting of PFO and PSO models to ΔE variations of TPU composite fibrous films exposed to air and 300 ppm acetone vapors. K_1, K_2, and R^2 values are listed in Table 1. For all samples in air, the PFO model showed better fit, indicating physical adsorption of moisture. Although R^2 values were similar for neat TPU, PFO still slightly outperformed. Under 300 ppm acetone vapor, all samples fit the PSO model better, suggesting chemical adsorption dominates the sensing mechanism in the presence of acetone vapors.

Fig. 5(d) shows the PFO and PSO fitting of ΔE changes in TPU-UiO-66-AgNC films exposed to varying acetone concentrations. The PSO model fit better at 25–200 ppm, especially at 25 ppm, though R^2 values were close. Initially, PSO dominated, indicating chemical adsorption, but as saturation approached, PFO became more accurate, suggesting subsequent physical adsorption of moisture. This indicates that chemically active sites were occupied first, followed by weaker physical interactions with ambient moisture. Fig. 5(e) illustrates that TPU-UiO-66-AgNC composite fibers adsorb acetone vapor through both UiO-66 and the TPU matrix, increasing the local refractive index near the fiber

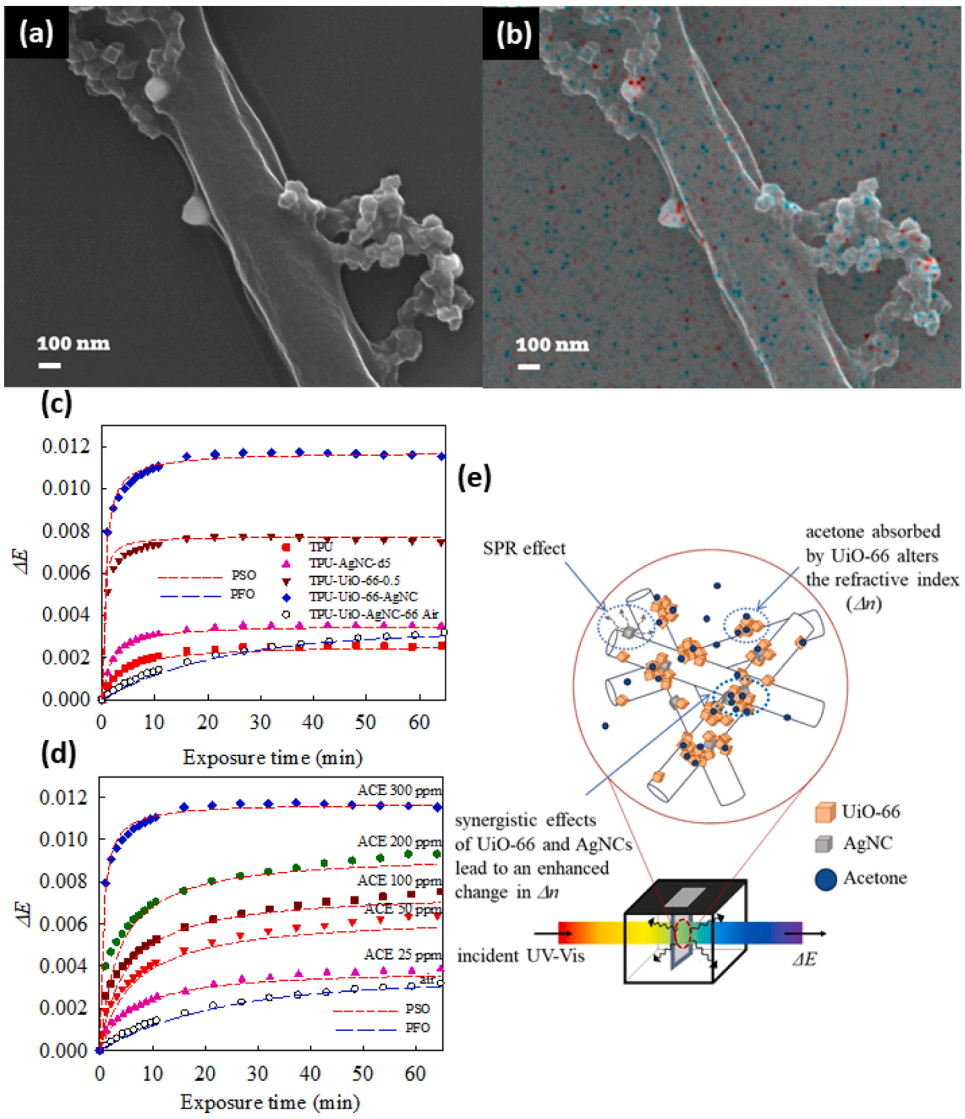

Fig. 5. (a) SEM of TPU fibers with anchored UiO-66 and AgNCs after ultrasonication and heating; (b) EDX mapping of Ag (red) and Zr (green) from (a); (c) ΔE of TPU composites exposed to 300 ppm acetone; (d) ΔE responses of TPU-UiO-66-AgNC films to varying acetone concentrations; (e) Schematic of proposed VOC sensing mechanism. ACE is the abbreviation for acetone.

surface. Randomly distributed AgNCs amplify this change via SPR, which is highly sensitive to the surrounding dielectric environment [42]. Although AgNCs are irregularly positioned around UiO-66 and along the fibers, TPU also contributes to acetone uptake. The resulting refractive index gradient enhances light scattering of incident visible light. This optical amplification, combined with SPR, leads to a synergistically increased extinction response, evidenced by greater UV–vis extinction changes in the composite films.

To investigate acetone adsorption, TPU-UiO-66 films were exposed to 300 ppm acetone vapor followed by a 1 h nitrogen purge. Pure water displays a broad O–H stretching band centered near 3300 cm^{-1}, while neat acetone exhibits weak peaks at 3615, 3520, and an overtone at 3414 cm^{-1}. Hydrogen bonding between acetone and water shifts these peaks to lower wavenumbers and introduces a new absorption band near 3250 cm^{-1} [43]. The FTIR peak at 3334 cm^{-1} (Fig. 6a) is thus attributed to water O–H stretching influenced by hydrogen bonding with acetone, contributing to the broad absorption in the 3600–3200 cm^{-1} range [43–45]. Furthermore, the observed shifts in C=O stretching-TPU (1706 → 1709 cm^{-1}) [46] and UiO-66 (1581 → 1582 cm^{-1}) [47] (Fig. 6b), indicating chemical interactions and enhanced acetone adsorption by surface-anchored UiO-66. These findings support the PSO model and prior reports of hydrogen bonding between UiO-66 and acetone [48].

The Table 2 summarizes VOC sensing performance across various electrospun composites fibers. Polymer type affects fiber diameter, which influences ΔE. PMMA fibers (~100–200 nm) offer high surface area but require UV-ozone activation to introduce functional sites for VOC adsorption. In co-electrospun PMMA systems, embedded nanoparticles interact effectively with VOCs, especially post-etching. CdSe–CdS quantum dots enhanced ΔE positively [20], while WO_3 induced negative changes. PMMA/AgNP/WO_3/SnO_2 composites achieved the best acetone sensitivity (20 ppm) [22], outperforming other PMMA-based systems [8,23].

TPU fibers (~1 μm) possess abundant C=O and N–H groups, enabling 300 ppm acetone detection without activation. However, nanoparticle functionality may be hindered by encapsulation. Ultrasonic anchoring of UiO-66 and AgNCs onto TPU surfaces enhances exposure. AgNCs exhibit strong SPR effects, boosting refractive index sensitivity. The resulting TPU-UiO-66-AgNC fibers show a 50 ppm detection limit and positive ΔE response, without the need for surface activation. These findings highlight how fiber morphology, surface treatment, and nanoparticle composition collectively influence VOC sensing performance. For comparison, polyacrylic acid @ thymol blue / cellulose nanocrystal

Table 1
Parameters associated with PFO and PSO kinetics models of TPU composite fibrous films for acetone vapor adsorption.

sample code		PFO model		PSO model	
		K_1 (min^{-1})	R^2	K_2 (ml^{-1} min^{-1})	R^2
TPU	air	0.121	0.98	236.914	0.95
	ACE 300 ppm	0.114	0.91	110.786	0.97
TPU-UiO-66-0.5	air	0.030	0.96	4.710	0.43
	ACE 300 ppm	0.200	0.71	507.401	0.94
TPU-AgNC-5d	air	0.097	0.93	441.898	0.69
	ACE 300 ppm	0.148	0.85	167.837	0.99
TPU-UiO-66-AgNC	air	*0.045*	*0.98*	*12.825*	*0.73*
	ACE 25 ppm	*0.078*	*0.93*	*44.890*	*0.97*
	ACE 50 ppm	*0.060*	*0.84*	*23.979*	*0.94*
	ACE 100 ppm	*0.053*	*0.75*	*27.247*	*0.96*
	ACE 200 ppm	*0.057*	*0.70*	*29.568*	*0.94*
	ACE 300 ppm	*0.179*	*0.71*	*149.103*	*0.99*

(PAA@TB/CNC) fibers with colorimetric response achieved the lowest detection limit (0.05 ppm) [49], reflecting the trade-off between sensor complexity and sensitivity.

To assess VOC responsiveness, ΔE of TPU-UiO-66-AgNC fibrous films were measured for polar (acetone, ethanol, IPA, THF) and nonpolar (*o*DCB, toluene) solvents (Fig. 7). While ΔE trends were similar at concentrations <100 ppm, their magnitudes varied. At high VOC levels (10,000 ppm), ΔE continued rising over time, likely due to slower evaporation or residual solvent droplets in the chamber.

Figures S6 shows PFO and PSO model fitting of ΔE changes in TPU-UiO-66-AgNC films exposed to 100 ppm VOCs, with K_1, K_2, and R^2 listed in Table S1. Ethanol, IPA, and toluene fit the PFO model better, while acetone, THF, and *o*DCB aligned more with PSO. These trends reflect interactions between TPU urethane groups [32], hydrophilic Zr clusters, and π–π interactions from UiO-66's BDC ligands with non-polar VOCs [16], as well as the influence of VOC molecular size. VOCs with ring structures, such as THF and *o*DCB, tend to exhibit lower ΔE values due to the mismatch between their molecular sizes and the pore size of UiO-66. For certain VOCs like IPA and THF, the R^2 values from both PFO and PSO model fittings were similar, suggesting that both physical and chemical adsorption may occur concurrently on TPU-UiO-66-AgNC composite fibrous films. Notably, VOCs that better fit the PFO model showed larger ΔE changes, likely due to multilayer physical adsorption on the fiber surface. These findings suggest that TPU-UiO-66-AgNC composite fibers exhibit distinct adsorption behaviors depending on the type of VOC being detected.

4. Conclusions

Electrospun TPU nanofibers were used for VOC detection via optical extinction changes. Composite fibrous films were prepared by two methods: co-electrospinning and ultrasonic oscillation. UiO-66 and AgNCs were anchored onto TPU fibers via ultrasonic treatment, resulting in a non-uniform surface distribution. Compared to co-electrospinning, ultrasonic treatment led to greater ΔE due to UiO-66 and AgNCs being exposed on the fiber surface rather than embedded under TPU chains. TPU-UiO-66 composites, especially with 0.5 wt % loading, showed enhanced acetone adsorption via UiO-66–VOC interactions, while TPU-AgNC-d5 exhibited SPR-enhanced extinction. The TPU-UiO-66-AgNC composite combined these effects, achieving a 50 ppm detection limit. Extinction changes followed PFO and PSO models, with stronger responses under PFO behavior. These results demonstrate the strong potential of TPU-UiO-66-AgNC films for sensitive acetone vapor sensing.

CRediT authorship contribution statement

Chien-Lin Huang: Writing – original draft, Project administration, Investigation, Funding acquisition, Conceptualization. **Yi-Chen Lin:** Visualization, Investigation, Formal analysis, Data curation. **Kai-Wun Chen:** Visualization, Investigation, Data curation. **Yin-Hsuan Chang:**

Table 2
VOC sensing performance across various electrospun composites fibers.

Electrospun Composite Fiber	Taget VOCs	Detect Mechanism	Surface Activation	Detection limit (ppm)	reference
P3HT/PMMA	acetone	extinction	-	500	[8]
PMMA/AgNP/CdSe−CdS	1-butanol	extinction	UV-ozone	100	[20]
PMMA/AgNP/SnO_2-WO_3	acetone	extinction	UV-ozone	100	[23]
PMMA/AgNP/WO_3/SnO_2	acetone	extinction	UV-ozone	20	[22]
PAA@TB/CNC	acetone	Colorimetric	-	0.05	[49]
TPU-UiO-66-AgNC	acetone	extinction	-	50	This study

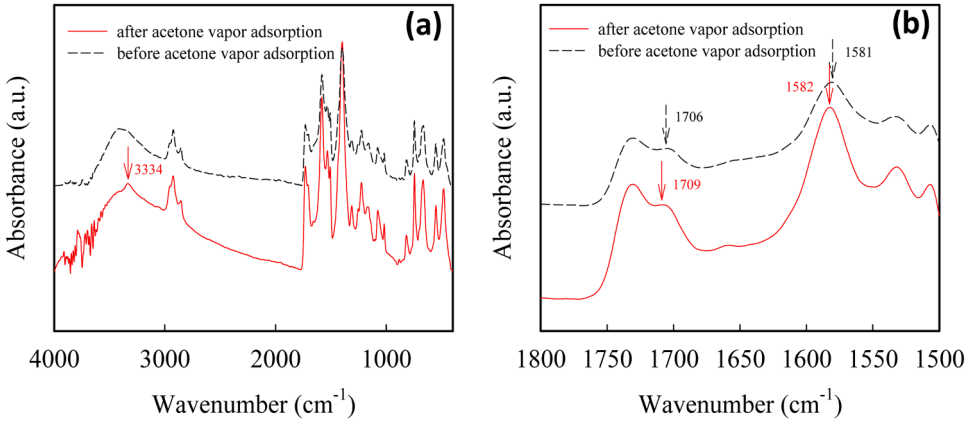

Fig. 6. (a) FTIR spectra of TPU-UiO-66 composite fibrous films before and after acetone vapor adsorption, and (b) the enlarged FTIR spectra in the 1800-1500 cm^{-1} range.

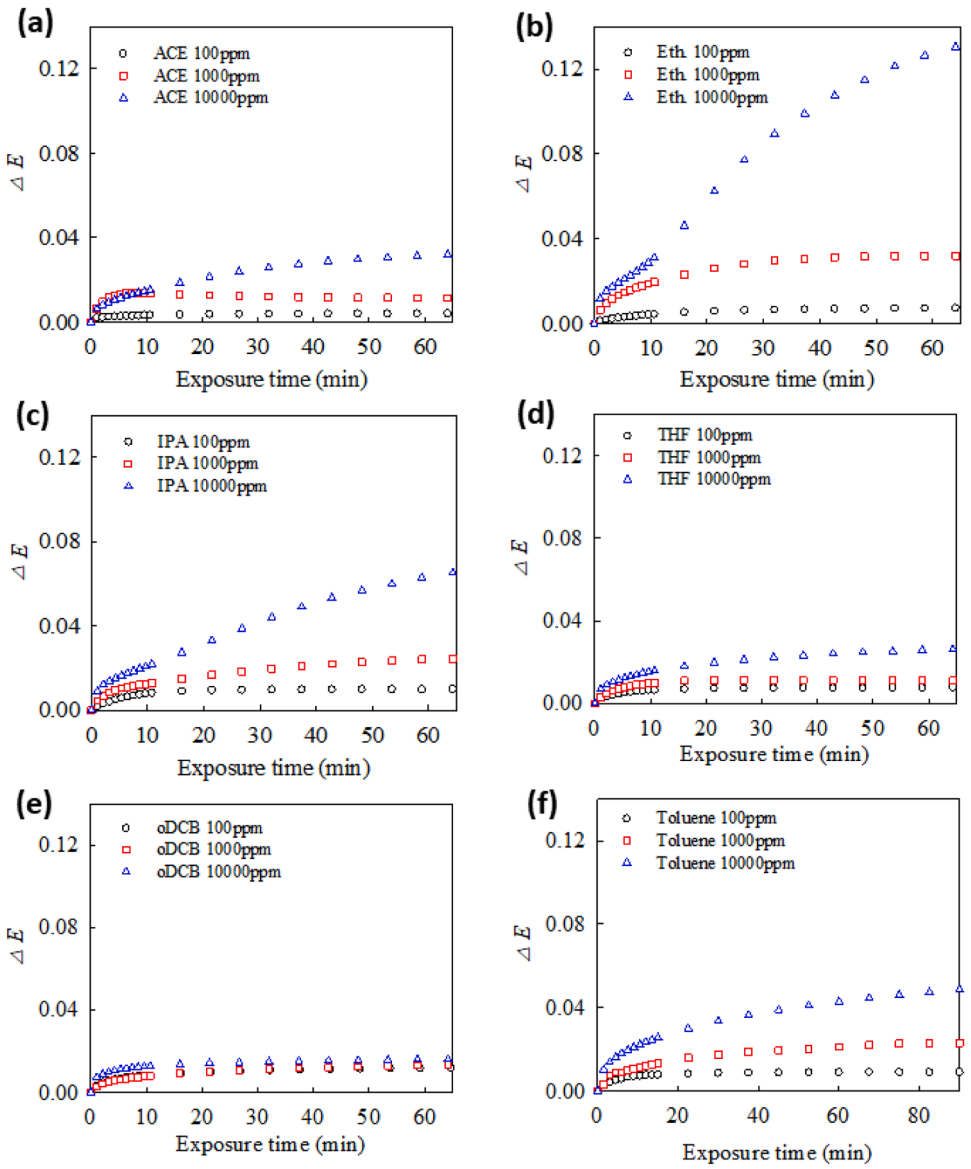

Fig. 7. extinction changes of the TPU-UiO-66-AgNC composite fibrous films exposed to various concentration of (a)acetone, (b) ethanol, (c) IPA, (d)THF, (e) *o*DCB, and (f) toluene with different time.

Writing – review & editing. **Ming-Chung Wu:** Methodology, Conceptualization. **Su-Wen Hsu:** Methodology, Conceptualization.

Declaration of competing interest

The authors declare that they have no known competing financial interests or personal relationships that could have appeared to influence the work reported in this paper.

Acknowledgments

The authors express their gratitude to the National Science and Technology Council of Taiwan for the research grants (NSTC 109-2221-E-035-032-) and to Feng Chia University for the research grant (23H00802) that supported this work. The authors also appreciate the Precision Instrument Support Center of Feng Chia University.

Supplementary materials

Supplementary material associated with this article can be found, in the online version, at doi:10.1016/j.surfin.2026.108933.

Data availability

Data will be made available on request.

References

[1] C. Wang, P. Sahay, Breath analysis using laser spectroscopic techniques: breath biomarkers, spectral fingerprints, and detection limits, Sens. (Basel) 9 (2009) 8230–8262, https://doi.org/10.3390/s91008230.
[2] V. Ruzsanyi, M. Peter Kalapos, Breath acetone as a potential marker in clinical practice, J. Breath. Res. 11 (2017) 024002, https://doi.org/10.1088/1752-7163/aa66d3.
[3] P. Fuchs, C. Loeseken, J.K. Schubert, W. Miekisch, Breath gas aldehydes as biomarkers of lung cancer, Int. J. Cancer 126 (2010) 2663–2670, https://doi.org/10.1002/ijc.24970.
[4] K. Schwarz, A. Pizzini, B. Arendacka, K. Zerlauth, W. Filipiak, A. Schmid, A. Dzien, S. Neuner, M. Lechleitner, S. Scholl-Burgi, W. Miekisch, J. Schubert, K. Unterkofler, V. Witkovsky, G. Gastl, A. Amann, Breath acetone-aspects of normal physiology related to age and gender as determined in a PTR-MS study, J. Breath. Res. 3 (2009) 027003, https://doi.org/10.1088/1752-7155/3/2/027003.
[5] N. Bhardwaj, S.C. Kundu, Electrospinning: a fascinating fiber fabrication technique, Biotechnol. Adv. 28 (2010) 325–347.

[6] Y.-W. Cheng, H.-A. Lu, Y.-C. Wang, A. Thierry, B. Lotz, C. Wang, Syndiotactic polystyrene nanofibers obtained from high-temperature solution electrospinning process, Macromolecules 43 (2010) 2371–2376, https://doi.org/10.1021/ma9025338.

[7] C. Feng, K.C. Khulbe, S. Tabe, Volatile organic compound removal by membrane gas stripping using electro-spun nanofiber membrane, Desalination 287 (2012) 98–102, https://doi.org/10.1016/j.desal.2011.04.074.

[8] M.-C. Wu, S.-H. Chan, T.-F. Lin, C.-F. Lu, W.-F. Su, Detection of volatile organic compounds using electrospun P3HT/PMMA fibrous film, J. Taiwan. Inst. Chem. Eng. 78 (2017) 552–560, https://doi.org/10.1016/j.jtice.2017.06.036.

[9] M.-C. Wu, C.-K. Kao, T.-F. Lin, S.-H. Chan, S.-H. Chen, C.-H. Lin, Y.-C. Huang, Z. Zhou, K. Wang, C.-S. Lai, Surface plasmon resonance amplified efficient polarization-selective volatile organic compounds CdSe-CdS/Ag/PMMA sensing material, Sens. Actuator B-Chem. 309 (2020) 127760, https://doi.org/10.1016/j.snb.2020.127760.

[10] J.-W. Yoon, J.-H. Lee, Toward breath analysis on a chip for disease diagnosis using semiconductor-based chemiresistors: recent progress and future perspectives, Lab. Chip. 17 (2017) 3537–3557.

[11] E. Scholten, L. Bromberg, G.C. Rutledge, T.A. Hatton, Electrospun polyurethane fibers for absorption of volatile organic compounds from air, ACS. Appl. Mater. Interfaces 3 (2011) 3902–3909, https://doi.org/10.1021/am200748y.

[12] Y. Wang, H. Tao, M. Chen, C. Chang, Core-sheath fiber—polyurethane guided solid particles grafted on polyacrylonitrile fiber surface and its application in adsorbing acetone, Microporous Mesoporous Mater. 308 (2020) 110252, https://doi.org/10.1016/j.micromeso.2020.110252.

[13] T. Terencio, F. Di Renzo, D. Berthomieu, P. Trens, Adsorption of acetone vapor by Cu-BTC: an experimental and computational study, J. Phys. Chem. C 117 (2013) 26156–26165, https://doi.org/10.1021/jp410152p.

[14] J.H. Cavka, S. Jakobsen, U. Olsbye, N. Guillou, C. Lamberti, S. Bordiga, K. P. Lillerud, A new zirconium inorganic building brick forming metal organic frameworks with exceptional stability, J. Am. Chem. Soc. 130 (2008) 13850–13851.

[15] U. Mueller, M. Schubert, F. Teich, H. Puetter, K. Schierle-Arndt, J. Pastré, Metal–organic frameworks—prospective industrial applications, J. Mater. Chem. 16 (2006) 626–636, https://doi.org/10.1039/b511962f.

[16] Y. Bai, Y. Dou, L.H. Xie, W. Rutledge, J.R. Li, H.C. Zhou, Zr-based metal-organic frameworks: design, synthesis, structure, and applications, Chem. Soc. Rev. 45 (2016) 2327–2367, https://doi.org/10.1039/c5cs00837a.

[17] R. Ou, W. Zhu, L. Li, X. Wang, Q. Wang, Q. Gao, A. Yuan, J. Pan, F. Yang, Boosted capture of volatile organic compounds in adsorption capacity and selectivity by rationally exploiting defect-engineering of UiO-66(Zr), Sep. Purif. Technol. 266 (2021) 118087, https://doi.org/10.1016/j.seppur.2020.118087.

[18] L.Q. Yu, F.H. Su, M.Y. Ma, Y.K. Lv, Metal-organic frameworks for the sorption of acetone and isopropanol in exhaled breath of diabetics prior to quantitation by gas chromatography, Mikrochim. Acta 186 (2019) 588, https://doi.org/10.1007/s00604-019-3713-1.

[19] W.L. Jhang, C.J. Li, A.S. Wang, C.W. Liu, S.W. Hsu, Tunable optical property of plasmonic-polymer nanocomposites composed of multilayer nanocrystal arrays stacked in a homogeneous polymer matrix, ACS Appl. Mater. Interfaces 12 (2020) 51873–51884, https://doi.org/10.1021/acsami.0c17170.

[20] M.C. Wu, C.H. Lin, T.H. Lin, S.H. Chan, Y.H. Chang, T.F. Lin, Z. Zhou, K. Wang, C. S. Lai, Ultrasensitive detection of volatile organic compounds by a freestanding aligned Ag/CdSe-CdS/PMMA texture with double-side UV-ozone treatment, ACS. Appl. Mater. Interfaces 11 (2019) 34454–34462, https://doi.org/10.1021/acsami.9b12333.

[21] Y. Kang, Y. Gong, Z. Hu, Z. Li, Z. Qiu, X. Zhu, P.M. Ajayan, Z. Fang, Plasmonic hot electron enhanced MoS 2 photocatalysis in hydrogen evolution, Nanoscale 7 (2015) 4482–4488.

[22] Y.-H. Chang, T.-H. Hsieh, K.-C. Hsiao, T.-H. Lin, K.-H. Hsu, M.-C. Wu, Electrospun fibrous nanocomposite sensing materials for monitoring biomarkers in exhaled breath, Polymers 15 (2023) 1833.

[23] T.-H. Lin, Y.-H. Chang, T.-H. Hsieh, Y.-C. Huang, M.-C. Wu, Electrospun SnO2/WO3 heterostructure nanocomposite fiber for enhanced acetone vapor detection, Polymers 15 (2023) 4318.

[24] Z. Pang, E. Yildirim, M.A. Pasquinelli, Q. Wei, Ammonia sensing performance of polyaniline-coated polyamide 6 nanofibers, ACS Omega 6 (2021) 8950–8957, https://doi.org/10.1021/acsomega.0c06272.

[25] M. Molco, F. Laye, E. Samperio, S. Ziv Sharabani, V. Fourman, D. Sherman, M. Tsotsalas, C. Woll, J. Lahann, A. Sitt, Performance fabrics obtained by in situ growth of metal-organic frameworks in electrospun fibers, ACS. Appl. Mater. Interfaces 13 (2021) 12491–12500, https://doi.org/10.1021/acsami.0c22729.

[26] W.-L. Jhang, M.-S. Huang, S.-W. Hsu, Unsymmetrical heterogeneous Au–Ag nanocrystals as catalysts, sensors, and drug carriers, ACS Appl. Nano Mater. 4 (2021) 10011–10017, https://doi.org/10.1021/acsanm.1c02866.

[27] J.J. Liu, Z.W. Jiang, S.W. Hsu, Investigation of the performance of heterogeneous MOF-silver nanocube nanocomposites as CO(2) reduction photocatalysts by in situ raman spectroscopy, ACS. Appl. Mater. Interfaces 15 (2023) 6716–6725, https://doi.org/10.1021/acsami.2c18510.

[28] B. Finnigan, P. Halley, K. Jack, A. McDowell, R. Truss, P. Casey, R. Knott, D. Martin, Effect of the average soft-segment length on the morphology and properties of segmented polyurethane nanocomposites, J. Appl. Polym. Sci. 102 (2006) 128–139, https://doi.org/10.1002/app.23347.

[29] I.M. Pereira, R.L. Oréfice, Study of the morphology exhibited by linear segmented polyurethanes, Macromol. Symp. 299-300 (2011) 190–198, https://doi.org/10.1002/masy.200900080.

[30] J.P. Theron, J.H. Knoetze, R.D. Sanderson, R. Hunter, K. Mequanint, T. Franz, P. Zilla, D. Bezuidenhout, Modification, crosslinking and reactive electrospinning of a thermoplastic medical polyurethane for vascular graft applications, Acta Biomater. 6 (2010) 2434–2447, https://doi.org/10.1016/j.actbio.2010.01.013.

[31] Y. Wang, H. Yang, Y. Xie, X. Bao, L. Pan, D. Zhao, J. Chen, M. Zou, T. Tian, R. Li, Strain effect on dielectricity of elastic thermoplastic polyurethanes, Polymers 16 (2024) 1465.

[32] X. Huang, Z. Huang, L. Zhang, R. Liu, Y. Lv, Highly efficient cataluminescence gas sensor for acetone vapor based on UIO-66 metal-organic frameworks as preconcentrator, Sens. Actuators B-Chem. 312 (2020) 127952, https://doi.org/10.1016/j.snb.2020.127952.

[33] X. Zhang, Y. Yang, W. Huang, Y. Yang, Y. Wang, C. He, N. Liu, M. Wu, L. Tang, g-C3N4/UiO-66 nanohybrids with enhanced photocatalytic activities for the oxidation of dye under visible light irradiation, Mater. Res. Bull. 99 (2018) 349–358, https://doi.org/10.1016/j.materresbull.2017.11.028.

[34] X. Zhang, X. Lv, X. Shi, Y. Yang, Y. Yang, Enhanced hydrophobic UiO-66 (University of Oslo 66) metal-organic framework with high capacity and selectivity for toluene capture from high humid air, J. Colloid. Interface Sci. 539 (2019) 152–160, https://doi.org/10.1016/j.jcis.2018.12.056.

[35] C. Zou, S. Vagin, A. Kronast, B. Rieger, Template mediated and solvent-free route to a variety of UiO-66 metal–organic frameworks, RSC Adv. 6 (2016) 102968–102971, https://doi.org/10.1039/c6ra23947a.

[36] J. Gao, M. Hu, Y. Dong, R.K. Li, Graphite-nanoplatelet-decorated polymer nanofiber with improved thermal, electrical, and mechanical properties, ACS Appl. Mater. Interfaces 5 (2013) 7758–7764, https://doi.org/10.1021/am401420k.

[37] R.D. Deshmukh, R.J. Composto, Direct observation of nanoparticle embedding into the surface of a polymer melt, Langmuir 23 (2007) 13169–13173.

[38] E.D. Revellame, D.L. Fortela, W. Sharp, R. Hernandez, M.E. Zappi, Adsorption kinetic modeling using pseudo-first order and pseudo-second order rate laws: A review, Clean. Eng. Technol. 1 (2020) 100032, https://doi.org/10.1016/j.clet.2020.100032.

[39] Y.-S. Ho, G. McKay, Pseudo-second order model for sorption processes, Process. Biochem. 34 (1999) 451–465.

[40] M. Lafuente, S. De Marchi, M. Urbiztondo, I. Pastoriza-Santos, I. Pérez-Juste, J. Santamaría, R. Mallada, M. Pina, Plasmonic MOF thin films with raman internal standard for fast and ultrasensitive SERS detection of chemical warfare agents in ambient air, ACS Sens. 6 (2021) 2241–2251, https://doi.org/10.1021/acssensors.1c00178.

[41] J. Lee, K. Lee, J. Kim, Fiber-based gas filter assembled via in situ synthesis of ZIF-8 metal organic frameworks for an optimal adsorption of SO(2): experimental and theoretical approaches, ACS Appl. Mater. Interfaces 13 (2021) 1620–1631, https://doi.org/10.1021/acsami.0c19957.

[42] X. Fan, W. Zheng, D.J. Singh, Light scattering and surface plasmons on small spherical particles, Light Sci. Appl. 3 (2014), https://doi.org/10.1038/lsa.2014.60 e179-e.

[43] J.-J. Max, C. Chapados, Infrared spectroscopy of acetone–water liquid mixtures. I. factor analysis, J. Chem. Phys. 119 (2003) 5632–5643, https://doi.org/10.1063/1.1600438.

[44] M. Takano, T. Takahashi, K. Iijima, Y. Yamada, The acetylacetone-water complex in a low-temperature solid argon matrix, J. Mol. Spectrosc. 333 (2017) 27–35, https://doi.org/10.1016/j.jms.2017.02.001.

[45] J.J. Max, C. Chapados, Infrared spectroscopy of acetone-water liquid mixtures. II. molecular model, J. Chem. Phys. 120 (2004) 6625–6641, https://doi.org/10.1063/1.1649936.

[46] D.K. Cha, A.A. Kloss, A.C. Tikanen, W.R. Fawcett, Solvent-induced frequency shifts in the infrared spectrum of acetone in organic solvents, Phys. Chem. Chem. Phys. 1 (1999) 4785–4790.

[47] Z. Qi, T. Qiu, H. Wang, C. Ye, Synthesis of ionic-liquid-functionalized UiO-66 framework by post-synthetic ligand exchange for the ultra-deep desulfurization, Fuel 268 (2020) 117336, https://doi.org/10.1016/j.fuel.2020.117336.

[48] J.J. Wardzala, J.P. Ruffley, I. Goodenough, A.M. Schmidt, P.B. Shukla, X. Wei, A. Bagusetty, M. De Souza, P. Das, D.J. Thompson, C.J. Karwacki, C.E. Wilmer, E. Borguet, N.L. Rosi, J.K. Johnson, Modeling of diffusion of acetone in UiO-66, J. Phys. Chem. C 124 (2020) 28469–28478, https://doi.org/10.1021/acs.jpcc.0c07040.

[49] X. Su, L. Wang, Y. Han, X. Xin, H. Yan, J. Cao, Cellulose nanocrystal/polyacrylic acid nanofiber composite aerogels characterized by 3D porous structure for colorimetric detection of breath acetone, Mikrochim. Acta 192 (2025) 679, https://doi.org/10.1007/s00604-025-07515-0.